

Photocatalytic decolorization of an azo dye employing TiO₂ anatase/brookite compounds obtained by hydrothermal methods

A. R. F. A. Teixeira¹, L. F. B. L. Pontes², I. M. G. dos Santos^{1*}

¹Universidade Federal da Paraíba, Núcleo de Pesquisa e Extensão, Laboratório de Combustíveis e Materiais, João Pessoa, PB, Brazil

²Universidade Federal da Paraíba, Departamento de Química, João Pessoa, PB, Brazil

Abstract

Titanium dioxide is a widely studied material with well-known applications for anatase and rutile phases. Moreover, brookite, another polymorph, which is more difficult to obtain, has caught scientific community interest, especially for photocatalysis applications. Among many methodologies for TiO₂ synthesis, the hydrothermal method stands out, with the possibility of controlling different parameters that lead to a specific phase composition, allowing selective polymorphic obtainment. This method was used to synthesize TiO₂ with different anatase/brookite ratios, by the use of different synthesis conditions as pH of the suspension, sodium salt concentration, and temperature, resulting in anatase-brookite photocatalyst with brookite composition ranging from 0 to 35%. The materials were characterized by X-ray diffraction, infrared spectroscopy, Raman spectroscopy, particle size measurement, and scanning electron microscopy. Photocatalysts with the highest brookite amount showed the best photocatalytic results for Remazol golden yellow (RNL) dye decolorization. Moreover, the short-range disorder also played an important role in photocatalytic behavior.

Keywords: titanium dioxide, brookite, anatase, photocatalysis, short-range disorder.

INTRODUCTION


Titanium dioxide has been applied in different fields, as photocatalysts, solar cells, electronic devices, and pigments. It is a chemically stable material, cheap, easy to prepare, and a non-toxic semiconductor. Among the natural occurring polymorphs, anatase and rutile are the most studied ones with different applications depending on the crystalline structure, while brookite is only obtained under specific conditions, and it has received more attention in the last decades [1]. Regarding environmental remediation applications, anatase has been far and wide applied especially as a catalyst for pollutants photodegradation, as well as its mixed framework with rutile. Anatase/rutile TiO₂ has been used as a model photocatalyst in studies involving degradation of dyes [2], drugs [3], pesticides [4], and cyanobacteria [5], as well as water disinfection [6, 7]. Brookite has also been reported as a promising material for degradation or decolorization of dyes [8-14] and degradation of other pollutants [10, 15-17], as well as for CO₂ reduction [18], drug degradation [19], either pure or in bicrystalline samples. Brookite and brookite-based materials have also been proven to effectively split [20] and oxidize [21] water.

It has been suggested by many authors that a mixed framework of titania material supplies an interface feature that affects charge carrier lifetimes thus improving photocatalytic activity. Some of the factors affecting the photocatalytic activity of each TiO₂ polymorph are the

trapping of photogenerated charge carriers in defects sites [1] and recombination dynamics [22]. Experimental studies have already reported that the depth of electron-traps in brookite are estimated to be deeper than in anatase but shallower than in rutile, and this moderate depth in brookite allows an increase in the lifetime of reactive charge carriers [23]. Studies involving the tuning of photocatalytic properties by adjusting synthesis conditions also claim the matter of short-range structural disorder evaluation in order to understand photocatalytic processes [24], which are known to be closely related to local defects in the materials [24-27]. According to Sato et al. [28], distorted octahedra have dipole moments that promote charge separation and favor the photocatalytic activity of indates (MIn₂O₄, M= Ca, Sr; AInO₂, A= Li, Na). Similarly, Kim et al. [26] showed that strain affects not only stabilized anatase phase but also introduced oxygen vacancies that favor the photocatalytic activity. Wu et al. [25] confirmed that surface distortion plays an important role during photocatalysis. For multiphase TiO₂, another important aspect to be regarded is the role of interface defects [29].

The lack of understanding of the conditions favoring the crystallization of brookite triggers new studies on this topic since it is believed that there is no one-fit-all strategy to obtain this polymorph [1, 30]. Pure brookite samples were obtained by the hydrothermal method starting from different titanium precursors such as titanates [12, 31, 32], titanium alkoxides [10, 33], hydride [18], or salts [19, 34-36], and soluble complexes previously synthesized [37]. Among the reported methodologies, many authors have commented on the role of the precursor chemistry solution for the obtainment of a specific phase composition [38].

*ieda@quimica.ufpb.br

 <https://orcid.org/0000-0002-3349-3994>

In this sense, the presence of F⁻ or Na⁺ ions [38], ClO₄⁻ and Cl⁻ anions in acidic media [39, 40], and even the effect of specific ligands on precursor titanium complexes [41] have been pointed out as fundamental conditions for brookite crystallization over anatase or rutile. For all these results, long-time reactions (24-72 h) with temperatures of 180 to 250 °C were required. An outstanding synthesis method is the microwave-assisted hydrothermal method. Comparative studies between conventional and microwave-assisted heating for TiO₂ synthesis showed that the use of the microwave can shorten the duration of the reaction from 2 days to 2 h and lower the temperature from 200 to 120 °C [42]. Indeed, Yoon et al. [43] obtained brookite with rutile traces after microwave hydrothermal treatment of TiCl₃ and butanol at 190 °C for 30 min. Morishima et al. [44] reported pure brookite obtained after microwave treatment at 200 °C for 5 min, starting from a previously synthesized water-soluble titanium complex.

In this sense, studies involving the synthesis of new materials and understanding their properties are critically important. In this work, some parameters were evaluated for brookite-anatase formation by the microwave-assisted hydrothermal method, which was chosen as a versatile, low-temperature synthesis methodology. The obtained materials were tested as catalysts for Remazol golden yellow dye (RNL) decolorization. Structural and morphological properties of the materials were evaluated and related to the photocatalytic activity.

EXPERIMENTAL

Catalyst synthesis and characterization: the synthesis of TiO₂ materials by the microwave-assisted hydrothermal method was performed initially based on the works of Nguyen-Phan et al. [45] and Jiao et al. [46] and then adjusted according to preliminary results. Titanium tetraisopropoxide (Sigma Aldrich, 97%), isopropanol (Tedia), sodium nitrate (Neon, R.G.), and sodium hydroxide (Tedia, 98%) were employed in the synthesis. In the procedure, 100 mL of an aqueous solution of NaOH and/or NaNO₃/NaCH₃COO were added to 100 mL of a solution containing titanium isopropoxide and isopropanol ([Ti]=6.26x10⁻² mol.L⁻¹) under stirring for 1 h. The suspension obtained was hydrothermally treated in

a microwave oven at 80-150 °C for 5 min. The product obtained was washed and dried at 100 °C for 8 h. Different conditions were evaluated as displayed in Table I. Some syntheses were also performed by the hydrothermal method in an electric oven at 200 °C for 72 h.

The prepared samples were characterized by X-ray diffraction (XRD), Fourier transform infrared spectroscopy (FTIR), Raman spectroscopy, UV-visible spectroscopy, particle size measurements, and scanning electron microscopy (SEM). XRD patterns were obtained with an XRD-6000 Shimadzu diffractometer employing CuKα radiation (λ=0.15406 Å), operated at 2 kVA, 30 V, and 30 mA. The analysis was performed with a 2θ range of 10-90°, a step size of 0.02°, and a step time of 2 s. The FTIR spectra were obtained with an IR Prestige-21 Shimadzu spectrometer by analysis of a pellet with a mass ratio of 1:100 of catalyst:potassium bromide (KBr) in transmittance mode with a spectral range between 400 and 2000 cm⁻¹. To obtain the Raman spectra, an inVia Renishaw spectrophotometer was used with a 20 mW Ar laser (518 nm), and the Raman shift was measured in the range between 50 and 1300 cm⁻¹. The UV-visible spectra were obtained using a UV-2550 Shimadzu spectrophotometer with a spectral range of 190-900 nm in diffuse reflectance mode; the Wood and Tauc method [47] was employed to graphically determine the band gap. Dynamic light scattering (DLS) was used to measure the particle size of the samples by measurement of an aqueous suspension of 0.5 g.L⁻¹ using the Zetasizer Nano equipment from Malvern. SEM images were obtained using Zeiss LEO 1430 equipment. For the samples composed by different TiO₂ polymorphic phases, the estimated contents of anatase and brookite were obtained according to the methodology described by Zhang and Banfield [48] for anatase-rutile-brookite samples and applied for materials composed only by anatase and brookite phases by Shen et al. [9], according to:

$$W_A = \frac{k_A \cdot I_A}{k_A \cdot I_A + k_B \cdot I_B} \quad (A)$$

$$W_B = \frac{k_B \cdot I_B}{k_A \cdot I_A + k_B \cdot I_B} \quad (B)$$

where W_A and W_B represent the weight fractions

Table I - Sample identification and synthesis conditions.

Sample	Method*	Synthesis conditions	Temperature
A	MO	NaNO ₃ 0.8 mol.L ⁻¹ , pH=10	80 °C
B	MO	NaNO ₃ 1.5 mol.L ⁻¹ , pH=6	80 °C
C	MO	NaNO ₃ 0.8 mol.L ⁻¹ , pH=6	130 °C
D	MO	NaNO ₃ 1.5 mol.L ⁻¹ , pH=10	130 °C
E	CH	NaNO ₃ 0.8 mol.L ⁻¹ , pH=6	200 °C
F	CH	NaCH ₃ COO 1.5 mol.L ⁻¹ , pH=6	200 °C

*MO: microwave-assisted; CH: conventional heating.

of anatase and brookite, respectively, I_A represents the integrated intensity of the (101) anatase peak ($2\theta=25.3^\circ$), I_B represents the integrated intensity of the (121) brookite peak ($2\theta=30.8^\circ$), K_A and K_B represent optimized coefficients, corresponding to 0.886 and 2.721, respectively.

Photocatalysis: photocatalytic tests were performed in a magnetic-stirred quartz reactor irradiated with two 9 W UVC Osram Puritec lamps with the main emission at 254 nm. A total of 60 mg of catalyst and 90 mL of 10 mg.L⁻¹ of Remazol golden yellow (RNL, Dystar) aqueous solution were employed in the reaction, with a temperature maintained at 27 °C. Aliquots of the solution were removed with a syringe at different irradiation times and centrifuged for 10 min at 5000 rpm to separate the catalyst. UV-vis spectroscopic analysis of the solution was performed in absorbance mode using the same equipment described above. Adsorption tests were also carried out, employing similar conditions but in the absence of light.

RESULTS AND DISCUSSION

Catalyst synthesis and characterization

The XRD patterns of the samples obtained by the hydrothermal method confirmed the crystallization of bicrystalline TiO₂ composed by anatase and brookite phases, according to the index files ICDD 71-1166 and 29-1360, respectively (Fig. 1). Comparison of the different XRD patterns of samples obtained by microwave heating indicated the decrease of crystallinity of the anatase phase with temperature increase, as displayed in Table II. This behavior was confirmed by the synthesis of one more sample, which was heated at 150 °C using microwave radiation, with higher Na⁺ concentration (1.5 mol.L⁻¹) and pH 10, which was amorphous. This behavior may be related to the dissolution-recrystallization process, which is very usual in this method when microwave heating is present. Amorphous samples were also obtained after hydrothermalization using sodium acetate as a precursor

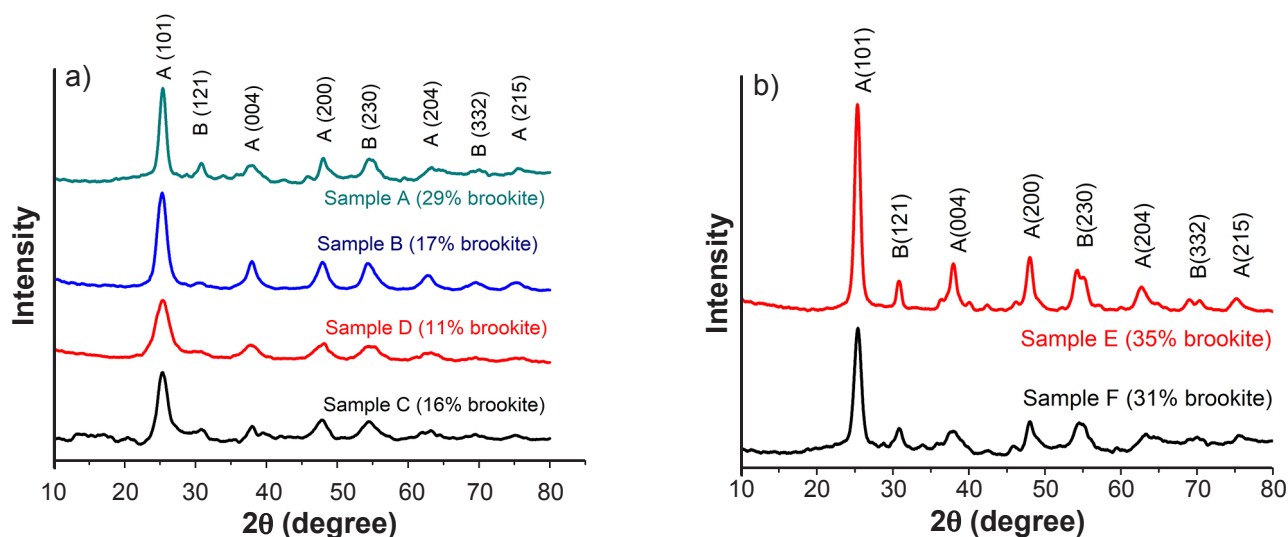


Figure 1: XRD patterns of samples obtained by hydrothermal method, using different heating sources: a) microwave; and b) conventional. Synthesis conditions of the samples are displayed in Table I. Phase indexing: A: anatase; B: brookite.

Table II - Results of peak deconvolution of the XRD patterns and the Raman spectra.

Sample	Particle size (nm)	Anatase			Brookite						
		XRD (101) reflection FWHM [#] (°)	RC* (%)	D** (nm)	Raman Peak (cm ⁻¹)	Raman FWHM [#] (cm ⁻¹)	XRD (121) reflection FWHM [#] (°)	RC* (%)	D** (nm)	Raman Peak (cm ⁻¹)	Raman FWHM [#] (cm ⁻¹)
A	248	1.58	74	5.17	516	54	1.39	92	5.95	316	55
B	333	2.08	78	3.92	519	94	2.23	77	3.70	317	69
C	312	1.96	100	4.16	517	80	1.97	66	4.19	317	66
D	259	1.51	88	5.42	517	42	2.20	100	3.75	317	70
E	355	1.05	53	7.82	519	51	1.12	25	7.40	320	31
F	194	1.21	66	6.75	517	45	0.77	29	10.82	320	31

[#] full width at half maximum; * relative crystallinity; ** crystallite size.

with microwave heating, as well as the sample prepared with sodium acetate at pH 10 with conventional heating. These data indicated that when acetate ion is present as a counterion in solution, crystallization may become more difficult. The long-range disorder was associated with the full width at half maximum (FWHM) of the main peak in the XRD patterns, as disorder leads to dislocation of the atoms/ions from equilibrium positions and broadens XRD peaks. Comparison between the two heating procedures also indicated that conventional heating led to samples with smaller crystallinity, but lower long-range disorder, for both anatase and brookite phases, as indicated by the smallest FWHM values displayed in Table II. Moreover, samples B and C obtained from suspensions with pH=6 had a higher long-range disorder for the anatase phase (bigger values of FWHM), compared to other samples obtained under microwave heating.

Particle size was determined by DLS measurements, considering the mean size of the cumulative curve (Table II).

Results did not have a correlation with particle size, probably due to sintering among particles. All samples showed a bimodal distribution curve, except sample E, which had a multimodal behavior. The second peaks in the distribution curves were due to agglomeration among particles, with a maximum value ranging from 4.2 to 5.6 μm , while the first peak ranged from 206 to 298 nm.

The infrared spectra of TiO_2 samples show a strong band ranging from 500-700 cm^{-1} depending on the polymorph, but for samples obtained in this work, as can be seen in Fig. 2, broad bands were observed and it was not possible to differentiate the vibration mode of each phase present. A band assigned to adsorbed water was identified at 1634 cm^{-1} for all of the samples, as well as a small band at 1170 cm^{-1} assigned to Ti-OH bonds.

Raman spectroscopy is pointed out as a sensitive tool to identify minor anatase impurity in the brookite phase [1, 49]. Brookite exhibits a complex Raman spectrum compared with the other natural polymorphs of TiO_2 , with

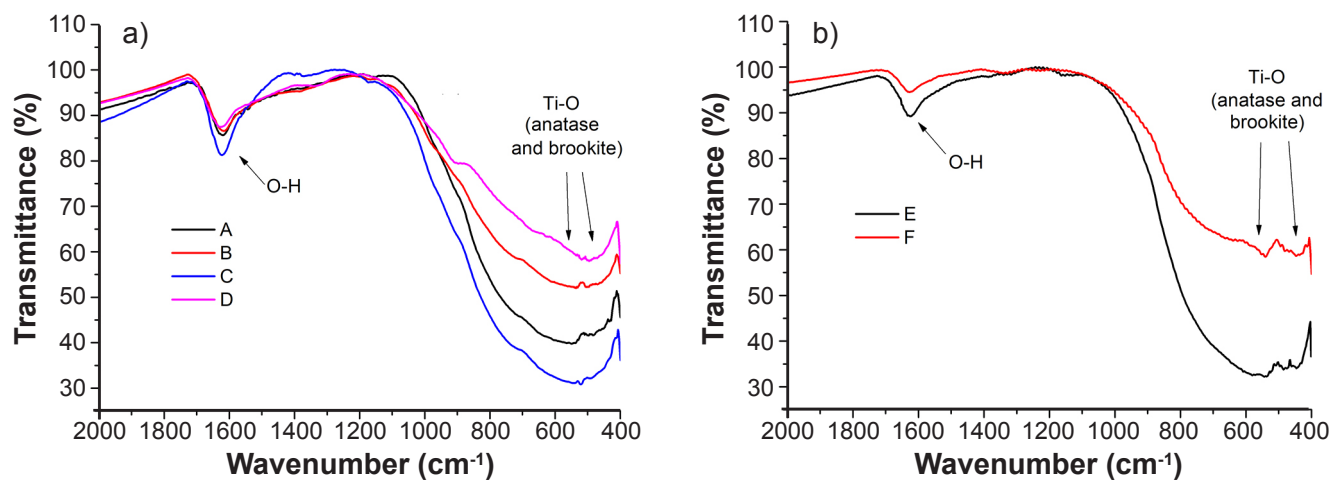


Figure 2: FTIR spectra of as-synthesized samples by hydrothermal method using different heating sources: a) microwave; and b) conventional.

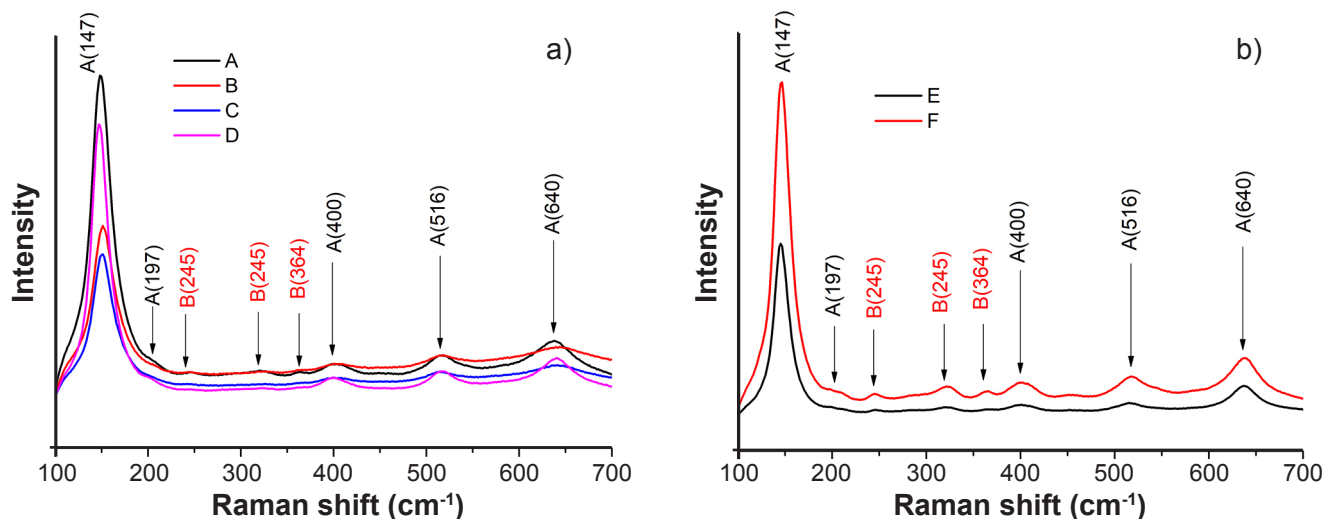


Figure 3: Raman spectra of as-synthesized samples by hydrothermal method using different heating sources: a) microwave; and b) conventional. Phase indexing: A: anatase; B: brookite.

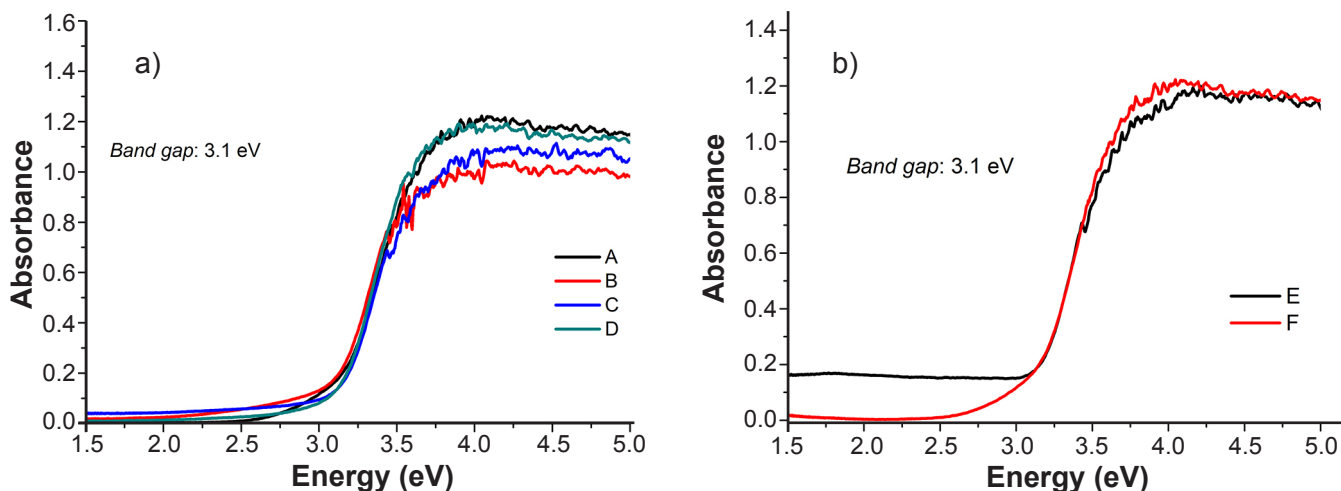


Figure 4: UV-vis spectra of samples synthesized by hydrothermal method using different heating sources: a) microwave; and b) conventional.

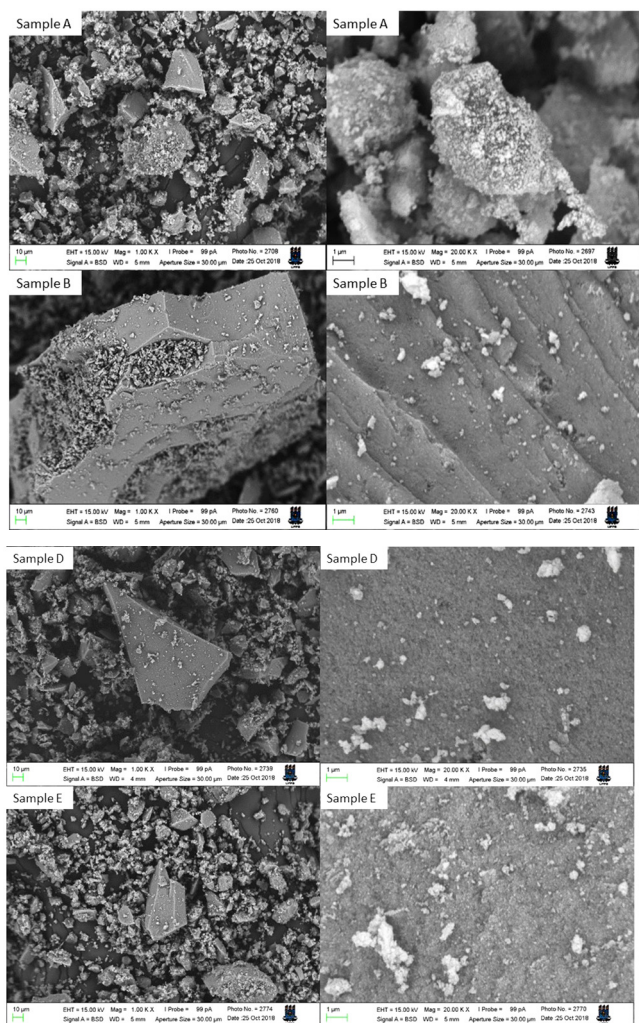


Figure 5: Backscattered electron images (SEM) at two magnifications of samples A, B, D, and E.

a very strong band at 153 cm^{-1} , a group of weaker bands at 195 , 247 , 322 , and 366 cm^{-1} , and another strong band at 636 cm^{-1} [50]. Anatase spectrum is simpler, with a very strong

band at 144 cm^{-1} , a weak band at 198 cm^{-1} , and broader bands at 400 , 516 , and 640 cm^{-1} [50]. It is worth noting that some of the brookite bands, especially the most intense one, can be overlapped with anatase signals, but the absence of a band at 516 cm^{-1} could confirm anatase is not present in a sample [49], while bands between 240 and 370 cm^{-1} confirm the presence of brookite. In Fig. 3, it was possible to identify bands assigned to the brookite phase in the samples with a higher brookite percentage estimated with XRD data. Similar profiles were obtained for the other crystalline samples. Similar to the XRD patterns, enlargement of the Raman peaks was associated with the short-range disorder, due to the dislocation of atoms/ions from equilibrium positions. The FWHM of the main peak assigned to anatase or brookite was calculated (Table II). According to Raman spectra, samples B and C had a higher short-range disorder, as indicated by the broad peaks and confirmed by the bigger FWHM values (Table II), especially for the anatase phase. This result was in agreement with a higher long-range disorder of these samples, indicated by the XRD patterns.

The band gap of the samples was determined employing the method reported by Wood and Tauc [47], using UV-visible spectra (Fig. 4). For all samples synthesized by the hydrothermal method, the band gap value was 3.1 eV and a very similar profile was observed for all of the samples.

Scanning electron microscopy (SEM) was also performed. Images obtained with backscattered electrons are displayed in Fig. 5. All samples were composed of small, agglomerated particles. While sample B displayed denser and bigger agglomerates, sample A seemed to have more loosely bonded particles.

Photocatalysis

All the TiO_2 samples were applied for Remazol golden yellow dye (RNL) aqueous solution decolorization. It is worth noting that the catalysts were able to decrease the intensity of all the RNL molecule absorption bands (Fig. 6), namely the main band related to the azo bond (maximum at

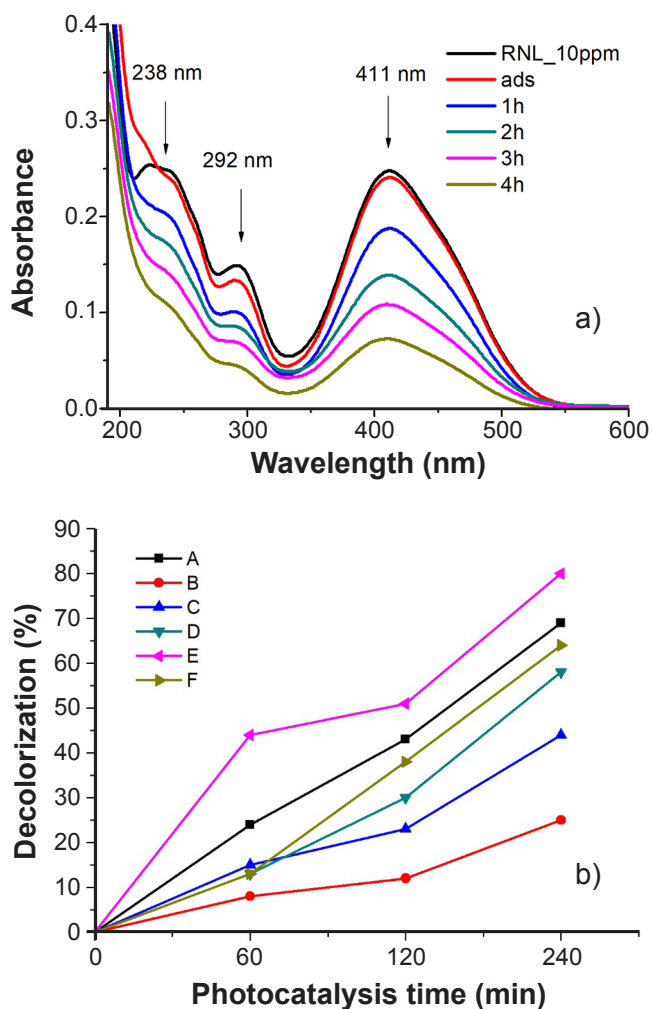


Figure 6: Results of: a) UV-visible spectra of RNL dye solution before and after photocatalysis with catalyst A (29% brookite); and b) catalysts performance for RNL decolorization over time.

411 nm) and those assigned to the aminoacetalinide group (maxima at 292 and 238 nm) [51]. Moreover, after adsorption tests, RNL spectra showed no meaningful change in the concentration even after 4 h of stirring with the catalysts in the dark. Percentages of decolorization for such tests ranged from 1% to 5% for samples obtained by microwave heating and from 3% to 8% for samples E and F obtained by conventional heating. These data were an indication of the catalyst's ability to promote the photodegradation of the dye molecules, and not only the decolorization of the solution, which takes place when the azo bond ($N=N$) is broken. Bicrystalline TiO_2 samples showed good photocatalytic activity, highlighting the samples obtained by microwave-assisted synthesis at $pH=10$; sample A with 29% content of brookite was able to promote 69% decolorization of the dye solution after 4 h of UVC irradiation (Fig. 6a), and sample D with 11% of brookite promoted 58% of decolorization. However, the best result was obtained with the catalyst synthesized by the traditional hydrothermal method (in an electric oven), with 31% of brookite (sample E), which achieved 80% of RNL solution decolorization after

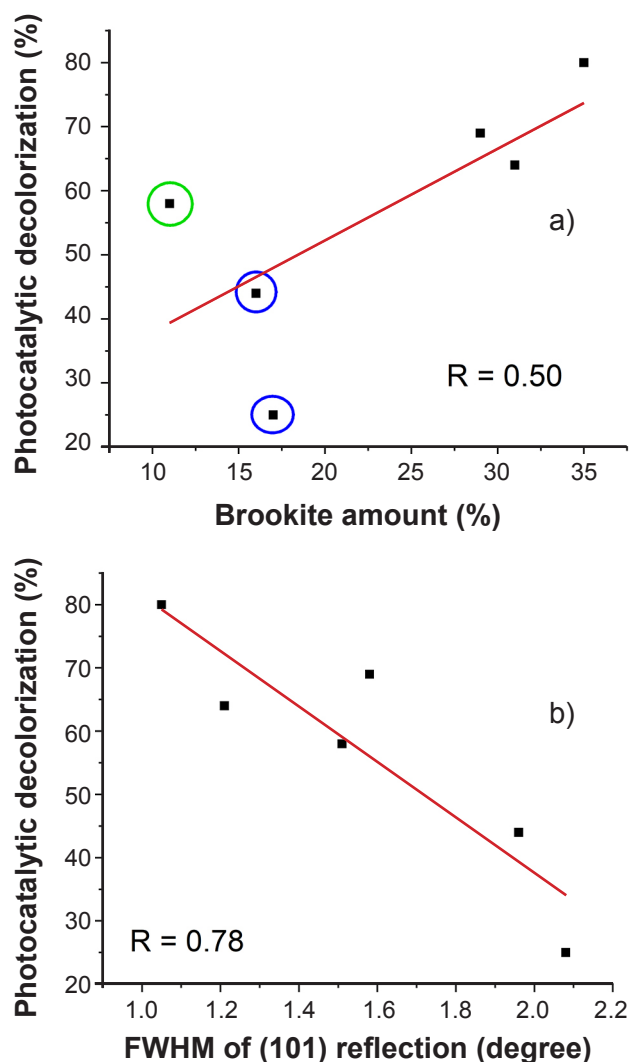


Figure 7: Correlation between photocatalytic efficiency and: a) brookite amount; and b) FWHM of the (101) reflection in the XRD patterns.

photocatalysis in the same conditions (Fig. 6b). Moreover, decolorization percentage was compared to structural and morphological data, displayed in Fig. 1 and Table II, and summarized in Fig. 7.

Particle size did not seem to correlate with the photocatalytic activity, as sample E had the biggest mean particle size and the greatest activity. Moreover, sample A had a bigger mean particle size and greater activity than sample F, which had the smallest mean particle size, even considering the position of the first peak in the particle size distribution curve. Three factors seem to be related to the photocatalytic activity of the bicrystalline samples: the short and the long-range disorder and the amount of brookite, as indicated by the data summarized in Fig. 7. The samples with the highest brookite contents were also the best catalysts for RNL decolorization in this study (Fig. 7a). Brookite has been pointed out as a promising material for photocatalysis [49] and has proven to be effective for CO_2 reduction [18, 52, 53], degradation of dyes [9, 12, 14, 54], drugs [19], and other pollutants [54]. In most of

these studies, samples composed of anatase and brookite were highlighted as the best photocatalysts compared to pure phase ones. The mixed structure, even for different phase combinations, such as anatase/rutile [29], is believed to affect charge carriers' transport and favor photocatalytic activity [17]. Tay *et al.* [55, 56] synthesized anatase-brookite photocatalysts and reported that brookite has a higher photocatalytic activity for water splitting due to the highest cathodic conduction band potential, which favors electron transfer to produce hydrogen. A similar effect should take place concerning O₂ reduction during photocatalysis in aqueous media. Moreover, the band edge positions of the different phases favor electron transfer from brookite to the anatase conduction band, which is slightly lower in energy, enhancing an effective electron-hole separation. Consequently, the electron transfer process due to interface can improve photocatalytic efficiency by decreasing recombination in mixed-phase materials.

In spite of the clear influence of brookite on the photocatalytic activity, this did not seem to be the only important factor influencing the photocatalytic activity. Samples B and C (marked with blue circles in Fig. 7a) had the lowest activity comparing to the other samples. Moreover, sample D (marked with a green circle in Fig. 7a) had a smaller amount of brookite (11%) compared to sample B (17%) and higher photocatalytic activity. According to the Raman spectra and XRD patterns, samples B and C had a remarkably high short-range disorder, as indicated by the broad peaks assigned to the anatase phase and small crystallites associated with a high long-range disorder (Fig. 7b). These data indicated that anatase/brookite materials may have smaller photocatalytic activity when a high short-range disorder is present. As anatase is a crystalline structure with highly distorted TiO₆ octahedra, a further increase of the short-range disorder induced by synthesis may form new mid gap states and favor the recombination of the photogenerated electron-hole pairs, decreasing the photocatalytic activity. As this sort of disorder leads to small symmetry changes, other techniques are necessary for more accurate characterization of the material.

CONCLUSIONS

Different synthesis conditions for the hydrothermal method were used to produce materials with similar phase composition, but with different amounts of anatase/brookite phases. This ratio was particularly important in photocatalytic activity, as samples with a greater amount of brookite displayed the greatest photocatalytic activity. Analysis of the Raman spectra indicated that this was the most important factor, but it was not the only one, as the short and long-range disorder clearly influenced the decolorization of the azo dye. For instance, a sample with a higher brookite amount may display a low photocatalytic activity if a high short-range disorder is present, as observed for two samples (B and C) synthesized by the microwave-assisted hydrothermal method.

ACKNOWLEDGEMENTS

This work was supported by PROINFRA/FINEP/MCTI, Fundação de Apoio à Pesquisa do Estado da Paraíba (Proc. 0012/2019 - FAPESQ/PB) and Coordenação de Aperfeiçoamento de Pessoal de Nível Superior - Brasil (CAPES) - Finance Code 001.

REFERENCES

- [1] M. Monai, T. Montini, P. Fornasiero, *Catalysts* **7** (2017) 304.
- [2] A. Khanna, V.K. Shetty, *Sol. Energy* **99** (2014) 67.
- [3] H.G. Oliveira, L.H. Ferreira, R. Bertazzoli, C. Longo, *Water Res.* **72** (2014) 305.
- [4] A.C. Affam, M. Chaudhuri, *J. Environ. Manage.* **130** (2013) 160.
- [5] L.X. Pinho, J. Azevedo, Â. Brito, A. Santos, P. Tamagnini, V.J.P. Vilar, V.M. Vasconcelos, R.R. Boaventura, *Chem. Eng. J.* **268** (2015) 144.
- [6] D. Rubio, J.F. Casanueva, E. Nebot, *J. Photochem. Photobiol. A Chem.* **271** (2013) 16.
- [7] I. García-Fernández, I. Fernández-Calderero, M.I. Polo-López, P. Fernández-Ibáñez, *Catal. Today* **240** (2014) 30.
- [8] H. Lin, L. Li, M. Zhao, X. Huang, X. Chen, G. Li, R. Yu, *J. Am. Chem. Soc.* **134** (2012) 8328.
- [9] X. Shen, B. Tian, J. Zhang, *Catal. Today* **201** (2013) 151.
- [10] M.J. López-Muñoz, A. Revilla, G. Alcalde, *Catal. Today* **240** (2015) 138.
- [11] V. Štengl, D. Králová, *Mater. Chem. Phys.* **129** (2011) 794.
- [12] B. Zhao, F. Chen, Q. Huang, J. Zhang, *Chem. Commun.* **34** (2009) 5115.
- [13] H. Xu, L. Zhang, *J. Phys. Chem. C* **113** (2009) 1785.
- [14] X. Shen, J. Zhang, B. Tian, *J. Mater. Sci.* **47** (2012) 5743.
- [15] R. Kaplan, B. Erjavec, A. Pintar, *Appl. Catal. A Gen.* **489** (2015) 51.
- [16] Z. Li, S. Cong, Y. Xu, *ACS Catal.* **4** (2014) 3273.
- [17] Y. Wang, C. Wang, X. Zhang, P. Sun, L. Kong, Y. Wei, H. Zheng, Y. Liu, *Appl. Surf. Sci.* **292** (2014) 937.
- [18] X. Xin, T. Xu, L. Wang, C. Wang, *Sci. Rep.* **6** (2016) 23684.
- [19] N. Tomic, M. Grujic-Brojcin, N. Fincur, B. Abramovic, B. Simovic, J. Krstic, B. Matovic, M. Scepanovic, *Mater. Chem. Phys.* **163** (2015) 518.
- [20] M. Cargnello, T. Montini, S.Y. Smolin, J.B. Priebe, J.J.D. Jaén, V.V.T. Doan-Nguyen, I.S. McKay, J.A. Schwalbe, M.M. Pohl, T.R. Gordon, Y. Lu, J.B. Baxter, A. Brückner, P. Fornasiero, C.B. Murray, *Proc. Natl. Acad. Sci. U.S.A.* **113** (2016) 3966.
- [21] A. Naldoni, T. Montini, F. Malara, M.M. Mróz, A. Beltram, T. Virgili, C.L. Boldrini, M. Marelli, I. Romero-Ocaña, J.J. Delgado, V. Dal Santo, P. Fornasiero, *ACS Catal.* **7** (2017) 1270.
- [22] B. Moss, K.K. Lim, A. Beltram, S. Moniz, J. Tang, P. Fornasiero, P. Barnes, J. Durrant, A. Kafizas, *Sci. Rep.* **7**

- (2017) 1.
- [23] J.J.M. Vequizo, H. Matsunaga, T. Ishiku, S. Kamimura, T. Ohno, A. Yamakata, ACS Catal. **7** (2017) 2644.
- [24] L. Chantelle, A.L.M. De Oliveira, B.J. Kennedy, J. Maul, M.R.S. Da Silva, T.M. Duarte, A.R. Albuquerque, J.R. Sambrano, R. Landers, M. Siu-Li, E. Longo, I.M.G. Dos Santos, Inorg. Chem. **59** (2020) 7666.
- [25] W. Wu, X. Xue, X. Jiang, Y. Zhang, Y. Wu, C. Pan, AIP Adv. **5** (2015) 1.
- [26] Y. Kim, M. Watanabe, J. Matsuda, A. Staykov, H. Kusaba, A. Takagaki, T. Akbay, T. Ishihara, J. Mater. Chem. A **8** (2020) 1335.
- [27] H. Xie, N. Li, X. Chen, J. Jiang, X. Zhao, Appl. Surf. Sci. **511** (2020) 145597.
- [28] J. Sato, H. Kobayashi, Y. Inoue, J. Phys. Chem. B **107** (2003) 7970.
- [29] R. Verma, S.K. Samdarshi, J. Alloys Compd. **629** (2015) 105.
- [30] S.G. Kumar, K.S.R.K. Rao, Nanoscale **6** (2014) 11574.
- [31] Y. Jiao, F. Chen, L. Zhang, E. Zhou, J. Zhang, Catal. Commun. **47** (2014) 32.
- [32] M.-H. Yang, P.-C. Chen, M.-C. Tsai, T.-T. Chen, I.-C. Chang, H.-T. Chiu, C.-Y. Lee, CrystEngComm **16** (2014) 441.
- [33] Z. Yang, B. Wang, H. Cui, H. An, Y. Pan, J. Zhai, J. Phys. Chem. C **119** (2015) 16905.
- [34] S.M. El-Sheikh, T.M. Khedr, G. Zhang, V. Vogiazzi, A.A. Ismail, K.O. Shea, D.D. Dionysiou, Chem. Eng. J. **310** (2016) 1.
- [35] Z. He, Y. Su, S. Yang, L. Wu, S. Liu, C. Ling, H. Yang, Sci. Bull. **61** (2016) 1818.
- [36] Y. Zou, X. Tan, T. Yu, Y. Li, Y. Li, R. Wang, L. Xue, Mater. Res. Bull. **80** (2016) 237.
- [37] A. Beltram, I. Romero-Ocana, J.J.D. Jaen, T. Montini, P. Fornasiero, Appl. Catal. A Gen. **518** (2016) 167.
- [38] H. Yang, F. Chen, Y. Jiao, J. Zhang, Chem. Eng. J. **214** (2013) 229.
- [39] N. Murakami, T. Kamai, T. Tsubota, T. Ohno, Catal. Commun. **10** (2009) 963.
- [40] N. Murakami, T. Kamai, T. Tsubota, T. Ohno, CrystEngComm **12** (2010) 532.
- [41] M. Yoshizawa, M. Kobayashi, V. Petrykin, H. Kato, M. Kakihana, J. Mater. Res. **29** (2014) 90.
- [42] F. Dufour, S. Cassaignon, O. Durupthy, C. Colbeau-Justin, C. Chanéac, Eur. J. Inorg. Chem. **2012** (2012) 2707.
- [43] S. Yoon, E.S. Lee, A. Manthiram, Inorg. Chem. **51** (2012) 3505.
- [44] Y. Morishima, M. Kobayashi, V. Petrykin, M. Kakihana, K. Tomita, J. Ceram. Soc. Japan **115** (2007) 826.
- [45] T.D. Nguyen-Phan, E.J. Kim, S.H. Hahn, W.J. Kim, E.W. Shin, J. Colloid Interface Sci. **356** (2011) 138.
- [46] Y. Jiao, B. Zhao, F. Chen, J. Zhang, CrystEngComm **13** (2011) 4167.
- [47] D.L. Wood, J. Tauc, Phys. Rev. B **5** (1972) 3144.
- [48] H. Zhang, J.F. Banfield, J. Phys. Chem. B **104** (2000) 3481.
- [49] A. Di Paola, M. Bellardita, L. Palmisano, Catalysts **3** (2013) 36.
- [50] G.A. Tompsett, G.A. Bowmaker, R.P. Cooney, J.B. Metson, K.A. Rodgers, J.M. Seakins, J. Raman Spectrosc. **26** (1995) 57.
- [51] M. Catanho, G.R.P. Malpass, A.J. Motheo, Quim. Nova **29** (2006) 983.
- [52] H. Zhao, L. Liu, J.M. Andino, Y. Li, J. Mater. Chem. A **1** (2013) 8209.
- [53] L. Liu, D.T. Pitts, H. Zhao, C. Zhao, Y. Li, Appl. Catal. A Gen. **467** (2013) 474.
- [54] B. Zhao, L. Lin, D. He, J. Mater. Chem. A **1** (2013) 1659.
- [55] Q. Tay, X. Wang, X. Zhao, J. Hong, Q. Zhang, R. Xu, Z. Chen, J. Catal. **342** (2016) 55.
- [56] Q. Tay, X. Liu, Y. Tang, Z. Jiang, T.C. Sum, Z. Chen, J. Phys. Chem. C **117** (2013) 14973.
- (Rec. 26/11/2020, Rev. 10/03/2021, 05/04/2021, Ac. 10/04/2021)